JOURNAL OF SOLID STATE CHEMISTRY **133,** 486–500 (1997)
ARTICLE NO. SC977516

Hydrogen Bonding and Jahn–Teller Distortion in Groutite, α-MnOOH, and Manganite, γ-MnOOH, and Their Relations to the Manganese Dioxides Ramsdellite and Pyrolusite

Thomas Kohler and Thomas Armbruster[1]

Laboratorium für chemische und mineralogische Kristallographie, Universität Bern, Freiestrasse 3, CH-3012 Bern,Switzerland

and

Eugen Libowitzky

Division of Geological and Planetary Sciences, California Institute of Technology, Pasadena, California 91125

Received December 16, 1996; in revised form June 18, 1997; accepted June 23, 1997

The crystal structures of groutite, α-MnOOH (space group *Pnma*, $a = 10.667(1)$, $b = 2.871(1)$, $c = 4.554(1)$ Å, $Z = 4$), and manganite, γ-MnOOH (space group $P2_1/c$, $a = 5.304(1)$, $b = 5.277(1)$, $c = 5.304(1)$ Å, $\beta = 114.38(2)^\circ$, $Z = 4$), both from the Kalahari manganese field (South Africa), were refined including hydrogen positions from room temperature X-ray single-crystal data. The refinements converged to *R* values of 1.5% for 479 (groutite) and of 2.0% for 821 (manganite) unique reflections, respectively. A (101) twin refinement based on F^2_{obs} was applied for manganite leading to a twin contribution of ca. 0.9 : 0.1. The structures of groutite and manganite are distorted derivatives of the MnO_2 polymorphs ramsdellite and pyrolusite (rutile structure), respectively. The structural distortions of the oxyhydroxides are caused by an interaction of Jahn–Teller distortion of octahedrally coordinated Mn^{3+} (four short and two long Mn–O distances) and hydrogen bonding. In both structures two symmetrically distinct O sites (O1 and O2) are three-coordinated by Mn^{3+}. The choice which O site forms an OH group is governed by the orientation of the Jahn–Teller distortion and space constraints dictated by the octahedral framework topology. The two long Mn–O bonds are formed by both O1 and O2 thus the Jahn–Teller distortion alone does not determine the preference of the OH group. In groutite, the OMn_3 coordination fragment which shows the strongest deviation from planarity toward a trigonal pyramid bonds to H where the O–H vector points perpendicular to the Mn_3 plane. In manganite the coordinations of O1 and O2 are very similar, thus H shows long range disorder as observed by twinning. Both, groutite and manganite have short O–H···O distances (2.6 Å) giving rise to peculiar IR absorption features between 3200 and 1800 cm^{-1}. Oriented single-crystal slabs of manganite and diaspore (isostructural to groutite) were studied by polarized FTIR spectroscopy at 82 and 298 K, and all H-bonding related IR-absorptions were assigned. Manganite, γ-MnOOH, and groutite, α-MnOOH, both transform in air above ca. 300°C to β-MnO_2 (pyrolusite) which was studied by *in situ* temperature dependent single-crystal X-ray diffraction. The topotactic relation is preserved during the transformation.

INTRODUCTION

The group of oxyhydroxides $M^{3+}OOH$ may be divided into two structural families; one with octahedral coordination and strong hydrogen bonds and another where *M* is seven-fold coordinated without strong hydrogen bonds. In the latter family of structures (M^{3+} = Ho, Tb, Yb, Lu, Er, Y) six oxygen atoms, three of which are hydroxyl groups, form a trigonal coordination prism around *M*, and the seventh O resides along a normal to a prism face closest to the *M* center. Oxyhydroxides with octahedrally coordinated *M* are found for M^{3+} = Al, Sc, Y, V, Cr, Mn, Fe, Co, Ni, Rh, Ga, and In. It is one of the characteristics of these compounds that various modifications exist, commonly labeled by a Greek letter as prefix. Unfortunately, the same prefix is used for different structure types depending on the chemical composition. Two modifications with octahedrally coordinated Mn^{3+}, groutite, α-MnOOH, and manganite, γ-MnOOH, are subject of this study. Both structures are composed of edge-sharing $Mn^{3+}O_6$ octahedra which are further linked to a three-dimensional framework by sharing vertices (Fig. 1). Edge-sharing single chains are found for derivatives of the rutile structure (e.g., manganite), whereas edge-sharing octahedral double chains are characteristic of α-AlOOH, diaspore; α-FeOOH, goethite; α-MnOOH, groutite. The same arrangement of octahedral double chains is

[1] To whom correspondence should be addressed.

0022-4596/97 $25.00

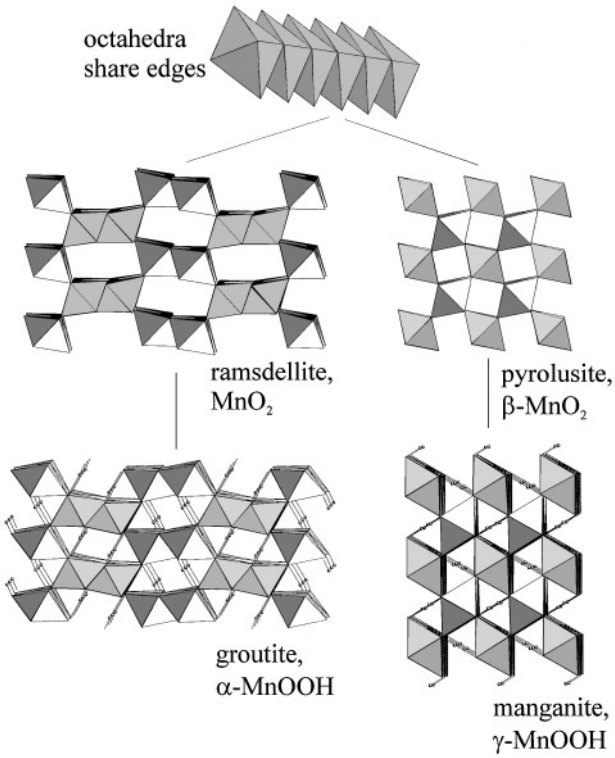

FIG. 1. Comparison of the arrangement of coordination octahedra in MnO_2 and MnOOH polymorphs. H atoms in MnOOH polymorphs are shown by small spheres with hydrogen bonds.

also known for MnO_2, ramsdellite (Fig. 1). Manganite, γ-MnOOH, possesses also a structurally related MnO_2 modification named pyrolusite, β-MnO_2 (rutile structure type; Fig. 1). Feitknechtite, β-MnOOH, a third modification, was not considered in this study because the structure is not well defined and suitable single crystals are not available.

Manganese dioxides and oxyhydroxides are of considerable importance in many technical applications. In alkaline batteries, for example, γ-MnO_2, related to the mineral nsutite, forms the basis due to specific physical and chemical properties. A detailed review on this subject is provided by Chabre and Pannetier (1). The structure of γ-MnO_2 has been described first as a random intergrowth of pyrolusite and ramsdellite layers (2) and was then shown to incorporate microtwinning defects (1). It has been proposed (3) that the second kind of defect does not occur in reduced MnOOH compounds, which means that reduction in batteries leads to a "de-microtwinning" of γ-MnO_2 and to the formation of an intergrowth of manganite and groutite. During the electrochemical processes, Mn^{4+} is partly reduced to Mn^{3+}, thus MnO_2 transforms to Mn_2O_3 or MnOOH. The mechanism of reduction may be different because the modifications show a wide range of phase boundaries and are able to absorb protons with only minor structural changes. New developments show that highly crystalline α-MnO_2 phases (hollandite-type) have high performances as electrode materials for secondary lithium cells (4).

The octahedral framework of manganite and pyrolusite is characterized by endless 1×1 channels (Fig. 1) where in manganite the hydrogen atoms reside. A rough structure model of manganite was proposed by Garrido (5) who considered manganite a marcasite-like structure. A subsequent structural reinvestigation showed that manganite is actually monoclinic and only pseudo-orthorhombic (6). The apparent orthorhombic symmetry is caused by polysynthetic twinning parallel to (101) in $P2_1/c$ setting. Dachs (7) derived the H position from a neutron diffraction study and showed the hydrogen bonding scheme. Isotopological[2] to manganite are InOOH and β-CrOOH. The hydrogen position in orthorhombic InOOH (space group $P2_1nm$, $a = 5.26$, $b = 4.56$, $c = 3.27$ Å) was determined by neutron diffraction (9), yielding a H arrangement different to manganite. β-CrOOH is isotypic to InOOH and has $a = 4.588$, $b = 4.292$, $c = 2.955$ Å (10).

In ramsdellite (11) and groutite (12) the connectivity of the double chains leads to 2×1 channels in the framework (Fig. 1) where in groutite the hydrogen atoms are located. Gruner (12) noted that groutite (α-MnOOH) is isostructural to goethite (α-FeOOH) and diaspore (α-AlOOH). A structure refinement neglecting H positions was performed attributing the large variations in Mn–O bond lengths to the Jahn–Teller effect (13). Using neutron diffraction Busing and Levy (14) located the H atom in diaspore, α-AlOOH, and noticed that the H atom is not on the connecting line of O atoms. Instead the OH bond makes an angle of 12.1(3)° with the O–O vector.

Since the most recent studies on groutite (13) and manganite (7), X-ray data acquisition and correction procedures have become significantly improved. In addition, structures of twinned crystals can be refined from single-crystal data. Thus, it was an aim of this paper to locate hydrogen atoms even in these transition metal oxyhydroxides with X-ray methods. The relatively short O–H···O distances (ca. 2.6 Å) in MnOOH polymorphs give rise to characteristic IR absorptions which are not yet well understood. Thus, oriented single-crystal IR absorption spectra were collected and interpreted. Furthermore, temperature dependent cell dimensions as well as topotactic relations between MnOOH

[2] Two crystals "have the same arrangement" and are isotypic (or isostructural) if their crystal structures are congruent with respect to space group and occupancy of equivalent positions (8). In principle, these structures (γ-MnOOH, InOOH, and β-CrOOH) are very similar concerning the arrangement of M^{3+} and O but not with respect to the hydrogen positions. In decision to this fact, these structures are called isotopological, a term often used in zeolite crystal chemistry.

and MnO_2 polymorphs were investigated by *in situ* high-temperature X-ray diffraction studies of groutite and manganite under oxidizing conditions.

EXPERIMENTAL

X-ray Data Collection and Structure Refinement

Manganite and groutite from the Nchwaning Mine in the Kalahari manganese field (Republic of South Africa) have end-member compositions, as verified by electron microprobe analyses. Selected crystals of manganite ($150 \times 100 \times 250$ μm) and groutite ($100 \times 70 \times 350$ μm) from this locality were mounted on glass fibers and transferred to an Enraf Nonius CAD4 diffractometer (graphite-monochromated Mo$K\alpha$ radiation) for structural study at room temperature. Experimental details for data collection and structure refinements are given in Table 1. Intensity data were empirically corrected for absorption (ψ scans). Data reduction, including background and Lorentz polarization corrections, was carried out using the SDP program library (15). Neutral atom scattering factors were used for the structure refinements.

Starting parameters for manganite refinements were adopted from Dachs (7) but the *B*-lattice setting was transformed to the primitive standard setting $P2_1/c$ using the transformation matrix $\frac{1}{2}0\frac{1}{2}$; $0\ -1\,0$; $-\frac{1}{2}0\,\frac{1}{2}$.

TABLE 1
Crystal and Refinement Parameters for Groutite and Manganite

	Groutite	Manganite	
Crystal size	$0.1 \times 0.07 \times 0.35$ mm	$0.15 \times 0.1 \times 0.25$ mm	
Space group	*Pnma*	$P2_1/c$	$B2_1/d$
a (Å)	10.667(1)	5.304(1)	8.915(1)
b (Å)	2.871(1)	5.277(1)	5.277(1)
c (Å)	4.554(1)	5.304(1)	5.748(1)
β (deg)		114.38(2)	90.02(1)
Z	4	4	8
Volume (Å^3)	139.47	135.2	270.4
Twinning contribution		0.9:0.1	
Data Collection and Refinement Parameters			
Scan type ω (deg) + 0.4 tan θ	1.5	1	
θ_{max} (deg)	40	42	
No. of measured reflections	3468	3378	
No. of unique reflections	494	876	
No. of observed reflections [$F_o > 4\sigma(F_o)$]	479	821	
No. of parameters	24	34	
R (%)	1.47	2.04	
R_w (%)	1.60		
wR_2 (%)		4.85	
Goof = *S*	1.7904	1.096	

Note. $R = (\sum|[F_{(obs)} - F_{(calc)}]|)/(\sum F_{(obs)})$;
$R_w = \{(\sum(\text{weight}|[F_{(obs)} - F_{(calc)}]|)^2)/(\sum(\text{weight}\,F^2_{(obs)}))\}^{1/2}$;
w$R_2 = \{[\sum\text{weight}(F^2_{(obs)} - F^2_{(calc)})^2]^2/[\sum\text{weight}(F^2_{(obs)})^2]\}^{1/2}$;
Goof $= \{(\sum(\text{weight}|[F_{(obs)} - F_{(calc)}]|)^2)/(\text{reflections}_{obs} - \text{parameters}_{(ref)})\}^{1/2}$.

A preliminary manganite refinement in space group $P2_1/c$ led to an *R* value of 4.8%. However, this result had to be disregarded because many symmetry forbidden reflections with highly significant intensities were observed. These reflections are due to (101) twinning as already noticed by Dachs (7). A second structure refinement based on F^2_{obs} with the program SHELXL93 (16) was performed for a twinned manganite model, resulting in an *R* value of 2.0%. The hydrogen position was determined from difference Fourier maps and subsequently refined. The largest residual peaks in these maps were ± 1.35 e/Å^3 surrounding the Mn atoms.

Groutite starting parameters were taken from Dent Glasser *et al.* (13) and refined with the program SHELXTL (17) using a $1/\sigma^2$ weighting scheme, converging at $R = 1.5\%$. The hydrogen position was determined from difference Fourier maps and subsequently refined. The largest residual peaks in these maps were ± 0.53 e/Å^3.

X-Ray Investigation of Manganite and Groutite at Elevated Temperatures

The same manganite crystal as used for the single-crystal data collection at room temperature was remounted on a SiO_2 glass fiber with a high temperature resistant resin. The specimen was transferred to the Enraf Nonius diffractometer equipped with a high temperature device where the crystal was heated by a temperature-controlled hot air stream. Starting at 25°C, the temperature was successively increased in steps of ca. 25 to 325°C. At each step, the temperature was kept constant for 1 h and the cell dimensions were refined. The crystal was kept for 18 h at 175°C to test the thermal stability.

This procedure was repeated with an additional groutite crystal ($200 \times 170 \times 350$ μm) which was heated up to 350°C. However, the thermal stability test at 175°C was not performed.

FTIR Spectroscopy

FTIR spectra were recorded on a Nicolet 60SX FTIR spectrometer using a glowbar light source, a KBr beam splitter, and a liquid nitrogen cooled MCT detector. For the low-temperature spectra (82 K) a commercial cryocell (MMR Technologies) with KBr windows was used. Polarized single-crystal spectra of manganite and diaspore were measured using a gold wire grid polarizer on AgBr substrate (extinction ratio at 2000 cm^{-1} ~1 : 100) and a sample aperture of 400 μm. For the measurements of an extremely small (<200 μm diameter) manganite (010) and diaspore (001) slab, and for testing of different, small manganite twin domains, a Nicplan FTIR microscope with a 15 × /0.58 N.A. cassegrain objective (Spectra-Tech Inc.) was employed. Spectra were recorded at a resolution of 2 cm^{-1} (4 cm^{-1}

with the microscope) and were averaged from 256 scans for the powder data and from at least 1024 scans for the single-crystal data.

Manganite and groutite powder samples were prepared by the conventional KBr pellet technique. However, since spectra from KBr powder pellets frequently show artifacts like impurities from trace amounts of water, surface OH groups, or organic substances, single-crystal samples were also prepared. Manganite and groutite crystals were oriented according to the morphology and cleavage of the crystals, whereas for diaspore, X-ray oriented, gem-quality crystal slabs from Shannon *et al.* (18) were available. The oriented and cut slabs were ground and polished on both sides until a final thickness of 2–6 μm was obtained. A detailed description of the polishing procedure is given by Libowitzky and Rossman (19). Due to the small size (only $\sim$300 μm) and perfect cleavage, thin groutite single-crystal slabs could not successfully be prepared, and thus the isotypic Al-oxyhydroxide was used.

RESULTS

X-Ray Structure Refinement of Groutite

The cell dimensions of groutite in space group *Pnma* are $a = 10.667(1)$, $b = 2.871(1)$, $c = 4.554(1)$ Å. Refined atomic coordinates and atomic displacement parameters are given in Table 2. Selected interatomic distances and angles for groutite are given in Table 3. The oxygen atoms form distorted octahedra around the manganese atoms. Four short Mn–O bonds form a rough square ($2 \times$ O1 1.895(1) and $2 \times$ O2 1.965(1) Å) while two long bonds, Mn–O1 (2.174(1) Å) and Mn–O2 (2.338(1) Å), complete the octahedron. The octahedral edges are shared to form double chains parallel to *b*. In the resulting tunnels, the hydrogen atom is bonded to O2 within 0.81(4) Å to form an OH group with a hydrogen bond to O1 within 1.82(4) Å.

X-Ray Structure Refinement of Manganite

Single-crystal X-ray data of manganite yielded the cell dimensions $a = 5.304(1)$, $b = 5.277(2)$, $c = 5.304(1)$ Å, $\beta = 114.38(2)^\circ$, and a (101) twin ratio of 0.9 : 0.1. Refined atomic coordinates and atomic displacement parameters are given in Table 2. Selected interatomic distances and angles for manganite are given in Table 3.

The structure of manganite consists of Mn octahedra sharing edges to form single octahedral chains. These chains are corner-linked (by O1 and O2) parallel to the *b*-axis to a three-dimensional framework. Mn^{3+} is bonded in a rough square twice to O1 with 1.977(1) and 1.982(1) Å and twice to O2 with 1.881(1) and 1.893(1) Å, respectively. Two additional long bonds, Mn–O2 (2.213(1) Å) and Mn–O1 (2.337(1) Å), complete the octahedron. The hydrogen position is located in the interstitial channels between the chains and bonds to O1 within 0.98(2) Å, thus forming an OH group. In addition, H forms a 1.61(2) Å hydrogen bond to O2.

Behavior of Manganite and Groutite at Elevated Temperatures

To elucidate the topotactic relation between manganite and pyrolusite the *B*-centered manganite cell setting (7), i.e. $B2_1/d$ with $a = 8.88$, $b = 5.25$, $c = 5.71$ Å, $\beta = 90.0^\circ$ is chosen because the cell orientation in this setting is the same as in pyrolusite (see Discussion). The twin contribution in manganite is not altered by heat treatment. This is confirmed by measuring the intensities of the $B2_1/d$ forbidden reflections characteristic of the twin which survive up to 300°C. At 325°C, no intensities for the current cell setting were found. A subsequent search of 20 strong reflections yielded a new orientation matrix and a distorted pseudotetragonal cell with $a = 4.409(7)$, $b = 4.421(3)$, and $c = 2.871(2)$ Å at 25°C. This cell is characteristic of distorted pyrolusite, β-MnO_2. In spite of the strong differences in cell

TABLE 2
Refined Atomic Coordinates and Atomic Displacement Parameters for Groutite and Manganite

Atom	*x/a*	*y/b*	*z/c*	U_{11}	U_{22}	U_{33}	U_{23}	U_{13}	U_{12}	U_{eq}
					Groutite, space group *Pnma*					
Mn	0.14014(1)	$\frac{1}{4}$	− 0.05014(3)	0.00696(9)	0.00534(9)	0.00620(9)	0	0.00099(4)	0	0.00616(5)
O1	− 0.18652(7)	$\frac{1}{4}$	0.2989(2)	0.0082(3)	0.0067(3)	0.0073(3)	0	0.0017(2)	0	0.0074(2)
O2	− 0.07017(7)	$\frac{1}{4}$	− 0.1947(2)	0.0087(3)	0.0076(3)	0.0058(3)	0	− 0.0001(2)	0	0.0074(2)
H2	− 0.099(3)	$\frac{1}{4}$	0.641(8)							0.038(8)
					Manganite, space group $P2_1/c$					
Mn	− 0.23684(3)	0.01033(3)	0.75464(2)	0.00451(8)	0.00564(8)	0.00477(9)	− 0.00056(3)	− 0.00209(5)	0.00070(3)	0.00492(6)
O1	0.3749(1)	0.1238(1)	0.6279(2)	0.0061(2)	0.0062(2)	0.0066(2)	− 0.0004(2)	− 0.0035(2)	0.0001(2)	0.0060(1)
O2	0.8752(1)	0.1256(1)	0.1206(2)	0.0058(2)	0.0067(2)	0.0064(2)	− 0.0008(2)	0.0030(2)	0.0007(2)	0.0062(1)
H1	0.284(4)	0.027(5)	0.725(4)							0.029(7)

TABLE 3
Selected Interatomic Distances (Å) and Angles (Deg) for Groutite and Manganite

Atom1	Atom2	Dist	A–O–B	Angle	
			Groutite		
Mn	O1	1.895(1)			
	O1	1.895(1)			
	O2	1.965(1)			
	O2	1.965(1)			
	O1	2.174(1)			
	O2	2.338(1)			
average	O	2.039			
O2	H2	0.81(4)	Mn–O2–H2	129(2)	
			Mn–O2–H2	112(1)	2×
			Mn–O2–Mn	101.80(3)	2×
			Mn–O2–Mn	93.86(3)	
O1	H2–O2	2.568(1)	Mn–O1–Mn	122.46(2)	2×
			Mn–O1–Mn	98.52(4)	
			O1–H2–O2	171(4)	
			Manganite		
Mn	O2	1.881(1)			
	O2	1.893(1)			
	O1	1.977(1)			
	O1	1.982(1)			
	O2	2.213(1)			
	O1	2.337(1)			
average	O	2.047			
O1	H1	0.98(2)	Mn–O1–H1	107(1)	
			Mn–O1–H1	109(1)	
			Mn–O1–H1	92(2)	
			Mn–O1–Mn	124.10(3)	
			Mn–O1–Mn	124.80(3)	
			Mn–O1–Mn	97.63(2)	
O2	H1–O1	2.595(1)	Mn–O2–Mn	126.86(3)	
			Mn–O2–Mn	125.75(3)	
			Mn–O2–Mn	94.65(2)	
			O1–H1–O2	178(2)	

dimensions between manganite and pyrolusite the transformation is of topotactic nature where the arrangement of octahedral chains remains preserved (Fig. 1). The most pronounced effect during heating of manganite is the increase of the *b*-axis from 5.277(1) Å at 25°C to 5.305(4) Å at 300°C (expansion of 0.5%), which after oxidation decreases to 4.421(3) Å for β-MnO_2 (contraction of 16%). The expansion of *a* and *c* of 0.2% and 0.1% between 25 and 300°C is less pronounced, and upon transformation $a/2$ of manganite contracts 1% whereas the contraction of $c/2$ is not significant.

The intensities of groutite characteristic X-ray reflections decreased strongly at 300°C and faded completely at 350°C. At 350°C only $0k0$ groutite reflections (equivalent to $00l$ reflections in pyrolusite) remained observed. A subsequent search for reflections at room temperature also yielded an angularly distorted pseudotetragonal unit cell ($a = b =$ 4.418(2), $c = 2.862(1)$ Å) characteristic of pyrolusite. However, the pyrolusite reflections were extremely smeared out in the omega directions leading to a half-width of ca. 4.5° for $hk0$ and 2.5° for $00l$ reflections, respectively. When groutite is heated, the *a*-axis increases from 10.665(2) Å at 25°C to 10.733(7) Å at 325°C (expansion of 0.6%) and at 350°C collapses to ca. $a/2 = 4.42$ Å (contraction of 17%), characteristic of *a* and *b* of pyrolusite. The expansion of *c* and *b* (0.3% and 0.2%) of groutite is less evident, and upon transformation these axes contract by 3% and 0.1%, respectively.

The oxidation of Mn^{3+} in manganite and groutite to Mn^{4+} in pyrolusite is accompanied by dehydration of the structure. In case of groutite, oxidation changes the arrangement of the octahedral framework but the orientation of the formerly 2×1 channels is maintained in the orientation of the 1×1 channels of pyrolusite. A list of cell dimensions with corresponding temperatures is given in Table 4 and shown in Figs. 2 and 3 for groutite and manganite, respectively.

TABLE 4
Cell Constants of Groutite and Manganite (*B*-Centered Setting) As a Function of Temperature

T (°C)	*a*	*b*	*c*
	Groutite, *Pnma*		
25	10.665(2)	2.866(2)	4.553(3)
50	10.671(2)	2.866(2)	4.554(3)
75	10.677(2)	2.867(2)	4.558(2)
100	10.682(3)	2.867(2)	4.559(3)
125	10.687(3)	2.868(2)	4.559(3)
150	10.693(2)	2.868(2)	4.560(3)
175	10.698(3)	2.869(2)	4.562(3)
200	10.699(3)	2.689(2)	4.562(3)
225	10.703(4)	2.870(2)	4.564(3)
250	10.712(3)	2.870(2)	4.564(3)
275	10.715(5)	2.871(3)	4.567(2)
300	10.719(7)	2.872(3)	4.566(4)
325	10.733(7)	2.873(3)	4.566(4)
% elongation	0.6	0.2	0.3
	Manganite, $B2_1/d$ setting, $\beta = 90.0°$		
25	8.195(1)	5.277(1)	5.748(1)
48	8.920(1)	5.282(1)	5.752(1)
75	8.923(1)	5.284(1)	5.754(1)
100	8.926(1)	5.287(1)	5.755(1)
125	8.926(1)	5.289(1)	5.755(1)
150	8.930(1)	5.290(1)	5.756(1)
175	8.930(1)	5.292(1)	5.756(1)
175 (18 h)	8.929(1)	5.292(1)	5.756(1)
200	8.931(1)	5.293(2)	5.757(1)
225	8.933(1)	5.296(2)	5.757(1)
250	8.934(1)	5.299(2)	5.759(1)
275	8.937(1)	5.303(2)	5.761(1)
300	8.937(2)	5.305(4)	5.759(2)
% elongation	0.2	0.5	0.1

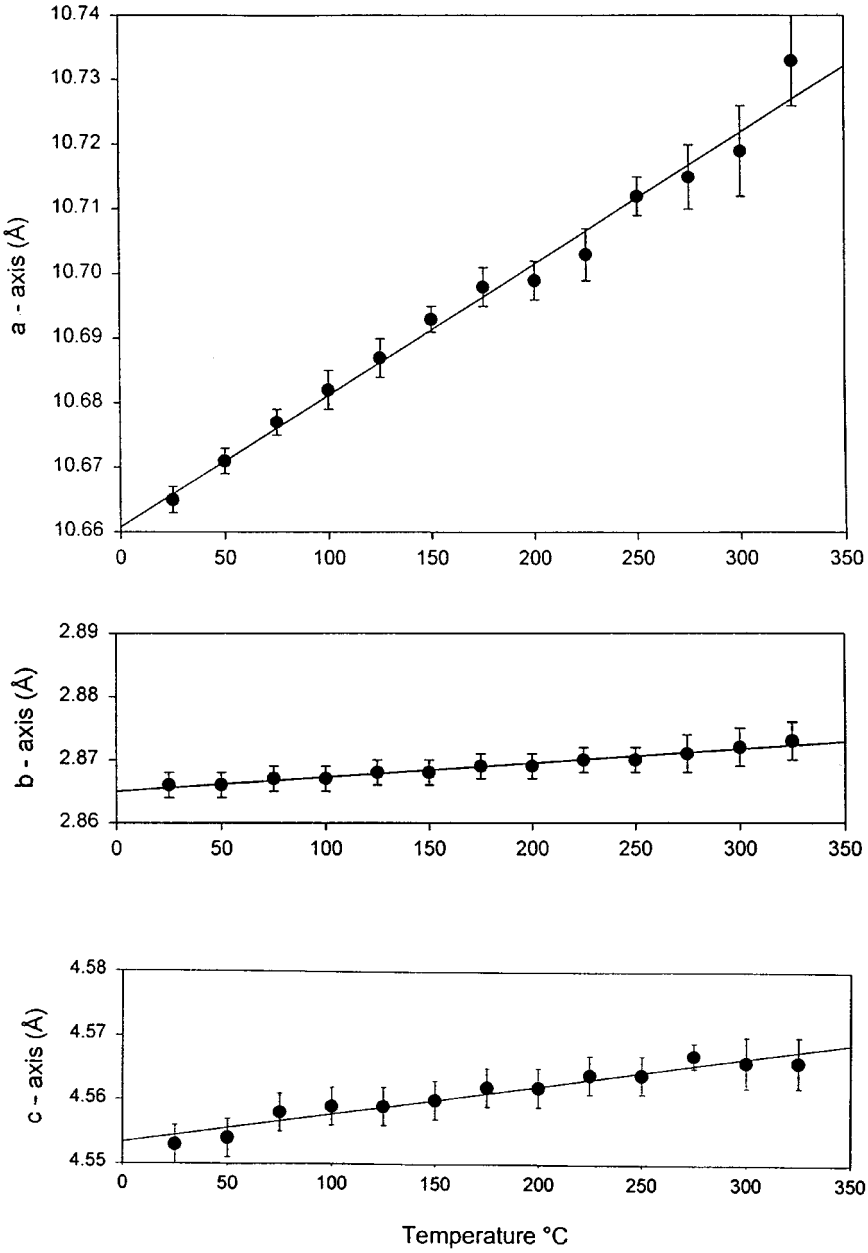

FIG. 2. Cell constants of groutite as a function of temperature.

FTIR Measurements on MnOOH Polymorphs

FTIR powder spectra of groutite and manganite at room and liquid nitrogen temperatures are presented in Figs. 4 and 5. A list of peak positions and band assignments is given in Table 5. Even though spectra of manganite and groutite have been published in previous papers (20, 21), the high accuracy of the FTIR spectroscopy (resulting in a revised list of peak positions), the acquisition of low temperature data, and, finally, the improved peak assignment in combination with the discussion of H bonds below, justify and moreover require the exhibition of the present data. In addition, the polarized spectra of manganite (Fig. 6) and diaspore single-crystals (Fig. 7; applicable also to groutite, goethite, etc.) facilitate an accurate band assignment and discussion.

For a complete factor group analysis of all IR-allowed modes of the OH groups (and their polarization behavior) in manganite and groutite, the VECTOR-tables (22) were used. In manganite, using the $B12_1/d1$ setting (factor group

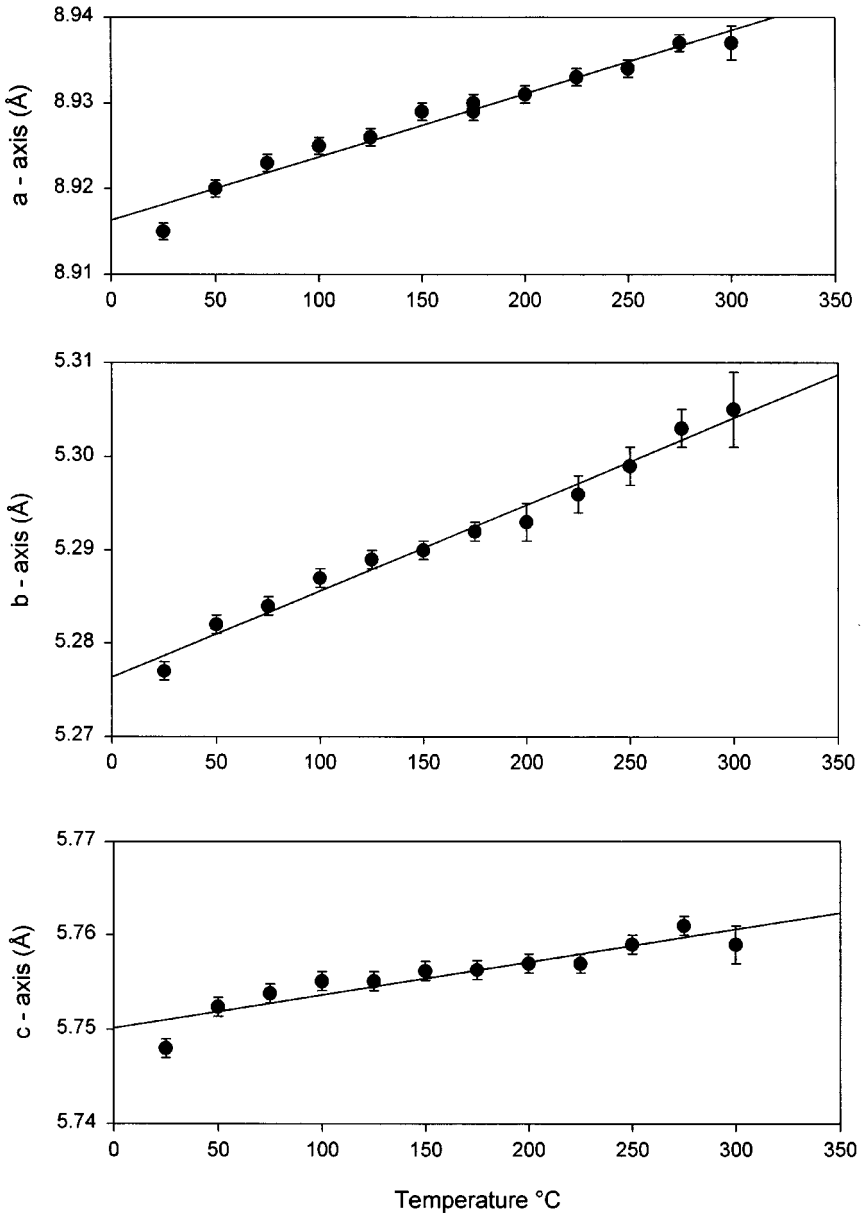

FIG. 3. Cell constants of manganite as a function of temperature.

C_{2h}), the OH stretching modes (ν) belong to species A_u (parallel to b) and B_u (parallel to a). The in-plane bending modes (δ), which are also parallel to the (001) plane, belong to species A_u and B_u with polarizations parallel to b and a. The out-of-plane bending mode (γ) is exactly perpendicular to the (001) plane and consequently belongs to species B_u parallel to c. The spectra of manganite and groutite show the following features: (a) A broad absorption band around 2600–2700 cm^{-1} which is polarized in the plane of the OH vectors. According to Novak (23) this frequency is in good agreement with an OH stretching mode belonging to a hydrogen bond with an O–H···O length of $\sim$2.60 Å (which is observed in manganite and groutite). (b) A single band in manganite and a double band in groutite around 2000 cm^{-1} shows the same polarization behavior. This interesting feature in the spectra will be the subject of the extensive discussion below. (c) The OH bending modes are observed around 1000–1150 cm^{-1}. According to the correlation diagrams (23), this frequency region is in good agreement with the frequencies of the stretching modes and the observed lengths of the H bonds. There are three bands in manganite and, on a first glance, only two in groutite. The lowest-energy band of this group is assigned to the γ mode (perpendicular to the OH vector plane), and the remaining

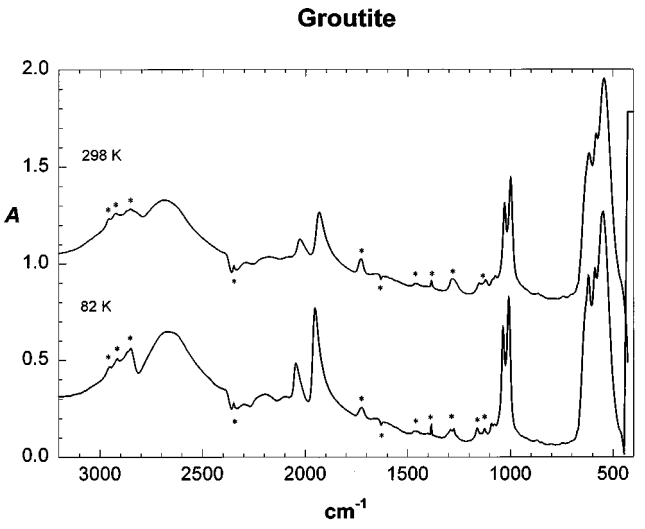

FIG. 4. FTIR powder spectrum of groutite at 82 and 298 K. Tiny spikes in the spectra which are caused by organic impurities, uncompensated water, and CO_2 are marked by asterisks.

TABLE 5
Peak Positions (cm^{-1}) of the Groutite and Manganite FTIR Powder Spectra (from Figs. 4 and 5) at 298 and 82 K

Groutite			Manganite		
298 K	82 K	Mode	298 K	82 K	Mode
2850	2855	3 γ,δ OH?	~2900	~2905	3γ,δ OH?
2686	2665	ν OH	2660	2627	ν OH
2026	2045	2 δ OH	2060	2083	2γ,δ OH
1932	1951	2 γ OH	—	—	—
—	—	—	1151	1160	δ1 OH
1027	1035	δ OH	1116	1124	δ2 OH
999	1008	γ OH	1086	1090	γ OH
618	621	l.m.	~638	~640	l.m.
582	587	l.m.	599	604	l.m.
544	549	l.m.	509	513	l.m.
~453	~458	l.m.	453	457	l.m.

Note. ESD's are $\pm 2\,cm^{-1}$, except where indicated by "~" (diffuse peak or shoulder). ν, stretching mode; δ, in-plane bending mode; γ, out-of-plane bending mode; l.m., Mn–O lattice mode; 2, first overtone; 3, second overtone.

two (manganite) or one (groutite) represent the δ modes in the OH plane. However, single-crystal spectra of diaspore show that there is also a second δ mode in the diaspore group spectra (parallel to *a*). The very weak appearance is explained by the OH vector orientation which is almost parallel to this axis. Hence, the bending mode (which is perpendicular to the vector) has almost no component parallel to that axis. (d) The lattice modes (Mn–O vibrations) are observed below $700\,cm^{-1}$.

In groutite (factor group D_{2h}) the OH vectors are aligned parallel to the (010) plane. Thus, ν belongs to B_{1u} (parallel to *c*) and B_{3u} (parallel to *a*). The in-plane bending modes belong to the same species, whereas for γ (which is perpendicular to that plane) only the B_{2u} mode (parallel to *b*) is active.

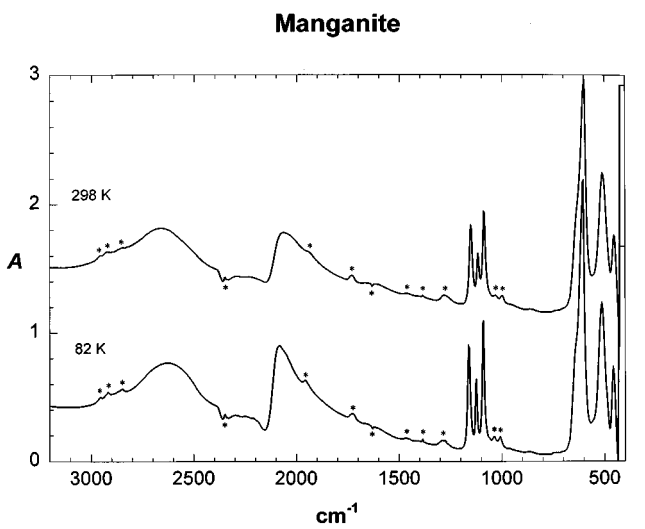

FIG. 5. FTIR powder spectrum of manganite at 82 and 298 K. Tiny spikes in the spectra which are caused by organic impurities, uncompensated water, and CO_2 are marked by asterisks.

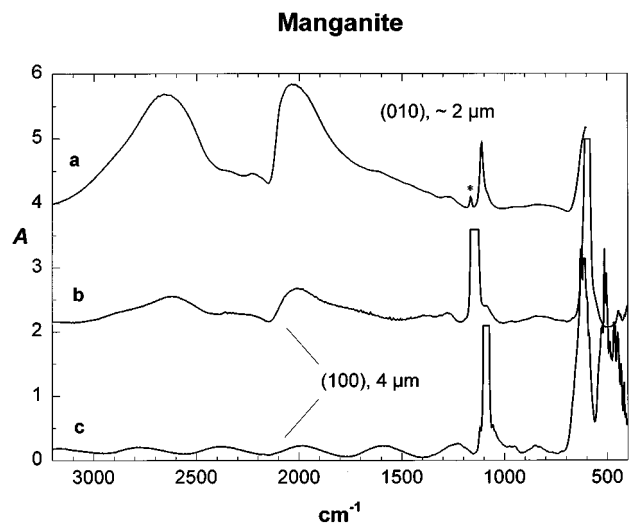

FIG. 6. Polarized FTIR spectra of manganite single-crystals. The asterisk marks a tiny spike in the "a" spectrum which belongs to the bending mode in *b* (caused by the conical light path connected with the high N.A. in the cassegrains of the FTIR microscope).

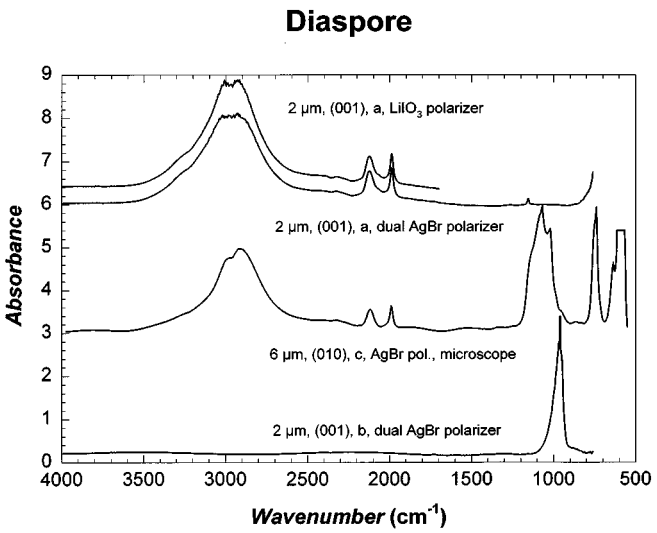

FIG. 7. Polarized FTIR spectra of diaspore single crystals. Sample thickness ~ 7 µm. Most of the high-intensity peaks are truncated.

DISCUSSION

Structure of Groutite

The structure of groutite, α-MnOOH, is a distorted derivative of ramsdellite, MnO_2, and is isostructural to diaspore, α-AlOOH (14), and goethite, α-FeOOH (24). The elongated $Mn^{3+}O_6$ octahedron (four short and two long Mn–O bonds) can be attributed to Jahn–Teller distortion and hydrogen bonding. To determine whether O1 or O2 is topologically preferred for an OH group, the OMn_3 fragments in groutite are studied (Fig. 8). The $O2Mn_3$ fragment shows the stronger deviation from planarity toward a trigonal pyramid than the $O1Mn_3$ fragment. The average Mn–O2–Mn angle is 99.15° ($2 \times 101.8°$ and 93.86°) in comparison to the average Mn–O1–Mn angle of 114.48° ($2 \times 122.46°$ and 98.52°). Therefore, H2 binds to O2, where the H2–O2 bond (0.81(4) Å) is perpendicular to the Mn_3 plane. Decreased O–H distances (0.8 Å versus ca. 1.0 Å) are characteristic of hydrogen positions derived from X-ray diffraction data where not the position of the nucleus but of the maximum electron density is refined. To fulfill bond valence requirements for Mn^{3+}, the OH group forms the longer Mn–O2 bond than the O1 site. Thus, the bond length distortion is influenced not only by the Jahn–Teller effect as Dent Glasser and Ingram (13) have pointed out but also by the hydrogen bonding of the OH group.

For diaspore, the angle between the vectors O2–H and O2–O1 of 12° can be explained by repulsion of the H^+ by Al^{3+} (14). A similar angle of 9(4)° was determined for groutite. If H would be on the line of oxygen centers, the Mn–O2–H2 angles had to be 141°, in contrast to the observed 129(2)°. Groutite and ramsdellite (11, 13) are not only

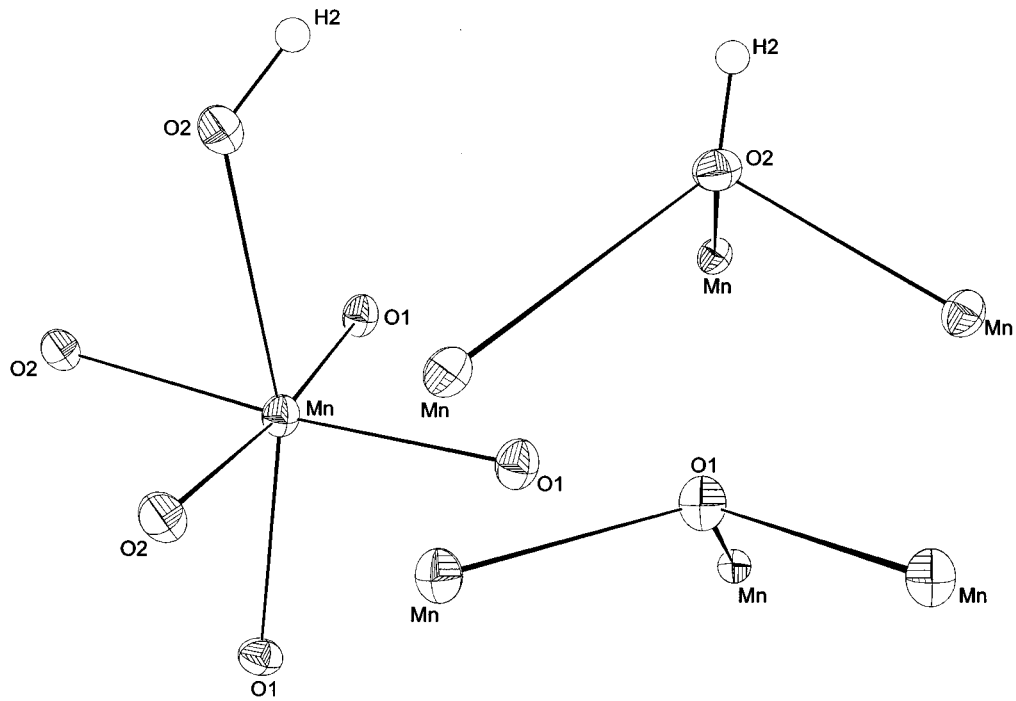

FIG. 8. The Mn^{3+} oxygen coordination in groutite. Atom displacement parameters are represented as 80% probability ellipsoids. Hydrogen is attached to O2 at the apex of the octahedron.

isotopological but also crystallize in the same space group. The 2×1 structural channels in ramsdellite have an almost rectangular cross-section whereas corresponding H-bearing channels in groutite are strongly distorted (Fig. 1). In addition, the angular distortion of the OMn_3 fragments is very similar in both structures. From this point of view one should expect a topotactic transformation between the two structures.

Structure of Manganite

Manganite, γ-MnOOH, is a distorted derivative of pyrolusite, β-MnO_2, isotypic with rutile (TiO_2). In the structure of pyrolusite (space group $P4_2/mnm$), the MnO_6 octahedron is slightly elongated with two long 1.894(1) Å and four short 1.882(2) Å Mn–O distances (25). Strongly elongated MnO_6 octahedra were found in manganite (Fig. 9) where the direction of elongation is the same as in pyrolusite. This enhanced structural distortion is caused by an interaction of the Jahn–Teller effect (Mn^{4+} is replaced by Mn^{3+}) and hydrogen bonding. Two symmetrically distinct O sites (O1 and O2) in manganite are three-coordinated by Mn^{3+}. However, on the basis of the deviation of the OMn_3 fragments from planarity (Fig. 9), no specific O site can be predetermined as preferred for OH. Both averages of OMn_3 angles lead practically to the same value (115.5° for O1 and 115.7° for O2).

To discuss the structural distortions and the ordered H arrangement in manganite, γ-MnOOH, we derive this structure from that of pyrolusite, β-MnO_2 (space group $P4_2/mnm$, $a = 4.4041$, $c = 2.8765$ Å (25)). The observed cell dimensions for manganite in the $B12_1/d1$ setting are $a = 8.915(2)$, $b = 5.277(2)$, $c = 5.748(2)$ Å, $\beta = 90.02(2)^\circ$ (standard space group setting is $P12_1/c1$). The above B-centered cell is related to pyrolusite by $a_{\text{pyrolusite}} = a/2_{\text{manganite}}$, $b_{\text{pyrolusite}} = b_{\text{manganite}}$, and $c_{\text{pyrolusite}} = c/2_{\text{manganite}}$ leading to an orthorhombic manganite subcell with $a = 4.458$, $b = 5.277$ and $c = 2.874$ Å. This subcell is sufficient to describe the Jahn–Teller distortion due to octahedral Mn^{3+} in manganite and obeys the space group $Pnnm$ (a nonisomorphic subgroup of $P4_2/mnm$) with Mn at ..2/m (0, 0, 0) and O at ..m (0.25, 0.375, 0). These coordinates lead to distorted MnO_6 octahedra with two long 2.27 Å and four short 1.93 Å Mn–O bonds. The structural channels running parallel to the c-axis may be described by edge-sharing chains of empty distorted O_6 octahedra which host the protons necessary for charge balance. Corresponding subcells were originally proposed for β-CrOOH and InOOH (26, 27) and for high pressure polymorphs of NiOOH, FeOOH, VOOH, RhOOH, and ScOOH (28). If the subcell with space group $Pnnm$ would describe the true symmetry of manganite and the other polymorphs cited above, the H atoms must either reside at $0, \frac{1}{2}, 0$, leading to two symmetric O–H distances of 1.295 Å, or H must be slightly displaced from the twofold axis ($0 + \Delta x, \frac{1}{2} + \Delta y, 0$) to form a covalent OH group with an O–H distance of ca. 1 Å and a strong hydrogen bond to the opposite O of ca. 1.59 Å. The latter arrangement would lead to H disorder. Brown (29) discusses the geometry of an

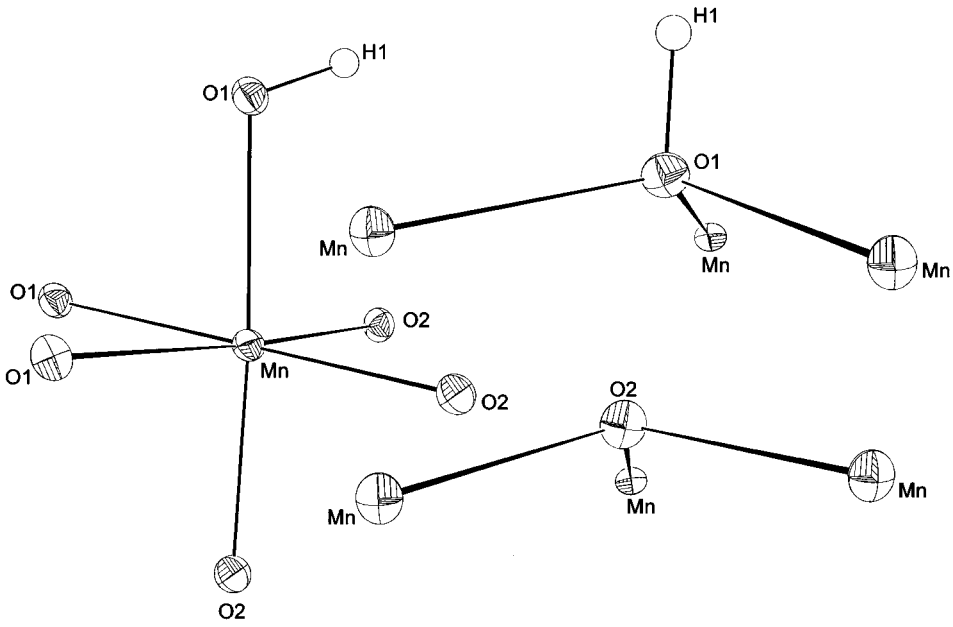

FIG. 9. The Mn^{3+} oxygen coordination in manganite. Atom displacement parameters are represented as 80% probability ellipsoids. Hydrogen is attached to O1 at the apex of the octahedron.

OH···O bond and shows that with an O–O distance of ca. 2.6 Å a symmetric hydrogen bond is not expected to occur. To avoid H disorder, the structure must further degenerate in symmetry, thus the twofold axis along *c* is no longer allowed. In turn, either one of the nonisomorphic monoclinic subgroups of *Pnnm* ($P2_1/n11$ or $P12_1/n1$, both $P2_1/c$, standard setting) or the acentric orthorhombic subgroups $Pn2_1m$ or $P2_1nm$ are expected. β-CrOOH and InOOH both crystallize in the latter orthorhombic subgroup (30, 10), while γ-MnOOH prefers a monoclinic cell (Fig. 10). For manganite, thus a cell setting different from the pseudo-pyrolusite cell has to be chosen in order to avoid a center of symmetry close to the supposed H position within the structural channel. In this new cell, all atoms are on general positions and no split H positions occur within the structural channels. Nevertheless the high *Pnnm* pseudosymmetry still exists, giving rise to long-range proton disorder which was analyzed in terms of twinning. The twinned domains are related to each other by a twofold axis parallel to the channel direction (*c*-axis in the pyrolusite cell or [101] in the manganite $P2_1/c$ cell). The twinning can also be described by a twin plane perpendicular to [101].

Behavior of Manganite and Groutite at Elevated Temperatures

If manganite is heated in air, the *a* and *b* lengths of the *B*-centered cell increase to a stronger degree than the *c* length. This indicates that the hydrogen bonds which are oriented parallel to (001) are weakened in this plane. Under

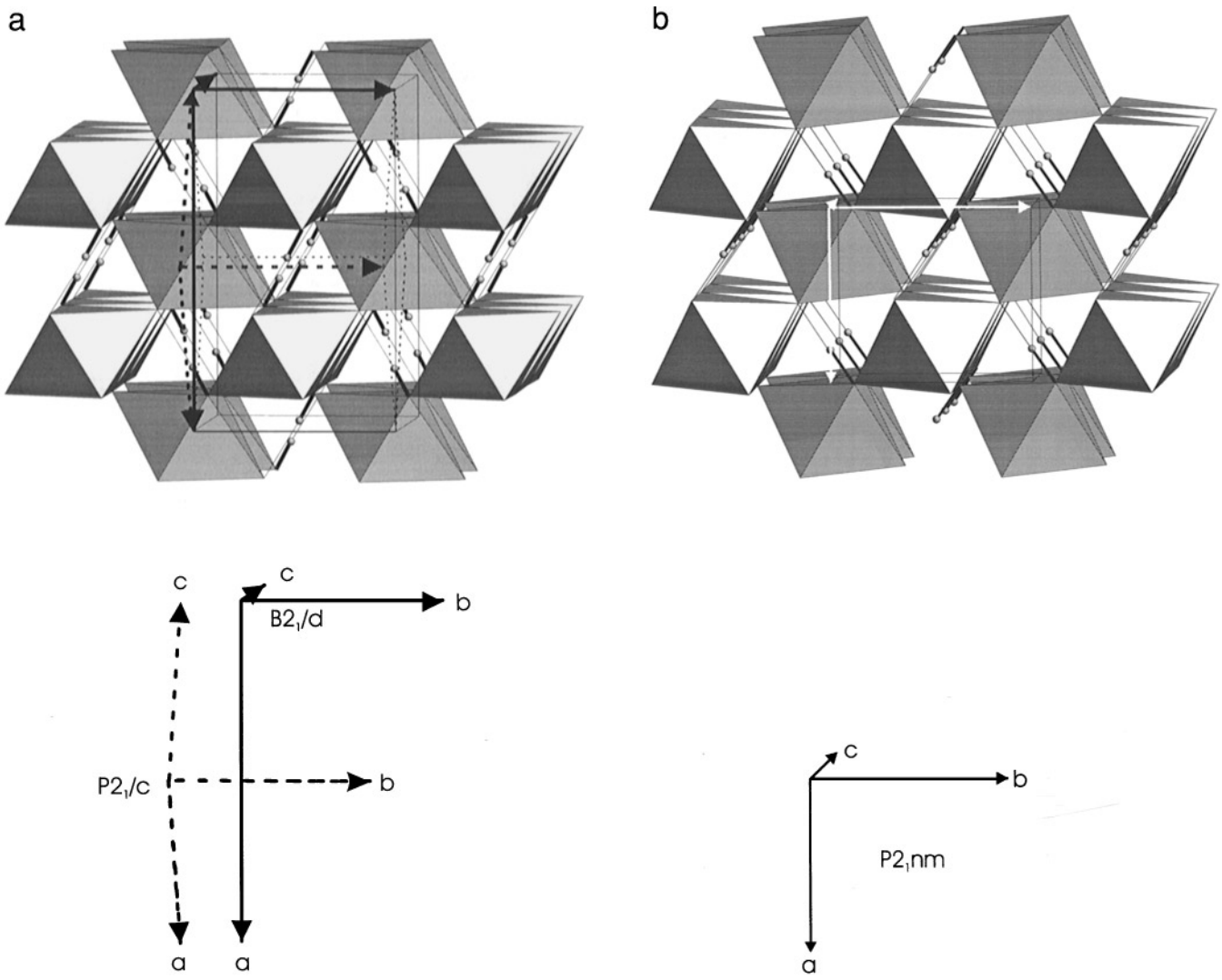

FIG. 10. Octahedral structural model of manganite (a) and InOOH (b), showing unit cell outlines and hydrogen position (small spheres) in the endless 1×1 channels.

air flush at 300°C manganite oxidizes within minutes to β-MnO_2, pyrolusite, where the orientation of the octahedral framework remains preserved. This observation confirms previous studies (31, 32). Due to the loss of H and oxidation to Mn^{4+}, the *b*-axis decreases strongly (16%) from 5.277 to 4.409 Å. This change is accompanied by the loss of the Jahn–Teller distortion and formation of square structural channels which were strongly distorted in manganite. The cell dimensions of pyrolusite deviate significantly from tetragonal symmetry which is caused either by strain due to the transformation or by the formation of orthorhombic pyrolusite (21). Deviation from tetragonal symmetry is well established for so-called secondary pyrolusite. On the basis of HRTM investigations it was proposed that manganite oxidizes to an intergrowth of β-MnO_2 and Mn_5O_8 responsible for the nontetragonal bulk properties (33). Champness (32) showed that the contraction of the *b*-axis during the transformation from manganite to pyrolusite involves formation of lamellar pores about 85 Å apart parallel to (010) in *B*-cell setting. Yamada *et al.* (34) confirmed these holes and also found ramsdellite domains in natural pyrolusite which formed as an oxidation product of manganite. The above statement that in our experiment manganite oxidized to pyrolusite should be taken with some caution. The recorded X-ray pattern is very diffuse, and the name pyrolusite was chosen because of very similar cell dimensions. Ripert *et al.* (35) have modeled the X-ray powder pattern of γ-MnO_2 by a random distribution of pyrolusite and ramsdellite layers. Up to ca. 15% ramsdellite contribution their calculated pattern is diffuse but still has the characteristics of pyrolusite.

The transformation of groutite to pyrolusite above 325°C under oxidizing conditions seems highly surprising because one would rather expect formation of the MnO_2 modification ramsdellite which is isotopological to groutite. However, previous studies (36–38) also obtained β-MnO_2 (pyrolusite) as oxidation product. Klingsberg and Roy (39) reported that in air groutite persists indefinitely below 130°C. At about 130°C it oxidizes partly to ramsdellite within two weeks; at 300°C it oxidizes within few hours. Above 300°C it transforms directly to pyrolusite. In a similar oxidation experiment of groutite at 300°C (36) additional weak and diffuse single-crystal X-ray spots indicated the presence of metastable Mn_2O_3 (hematite structure type) intergrown with pyrolusite. The formation of pyrolusite indicates that the linkage of octahedral chains is altered leading to 1×1 channels which may be explained by two different mechanisms. Lima-de-Faria and Lopes-Vieira (36) proposed a transformation mechanism where Mn migrates via octahedral interstices, while the oxygen arrangements remains preserved. In addition, slip planes responsible for the transformation were suggested (40).

IR-spectroscopic investigation of ramsdellite, MnO_2, has disclosed a single crystallographically-ordered H_2O molecule (21). Furthermore, ramsdellite used for a structural investigation (11) contained 1.3 wt% H_2O. Thus it was suggested that H_2O is an integral part of the ramsdellite structure (21). The high temperature transformation of groutite directly to pyrolusite without intermediate ramsdellite seems to confirm this assumption. However, as already discussed for the manganite–pyrolusite transformation, the existence of ramsdellite domains within pyrolusite can not be excluded.

The transformation from groutite ($V = 139.5$ Å^3) to pyrolusite ($2V = 111.6$ Å^3) is accompanied by a volume contraction of 20%, whereas the transformation from manganite ($V = 135.2$ Å^3) to pyrolusite causes a volume contraction of 17%. On the other hand, the transformation from groutite to structurally related ramsdellite ($V = 120.4$ Å^3) causes a volume reduction of ca. 14%. There is strong evidence that in transformations from MnOOH to MnO_2 the close packed oxygen framework does not remain preserved as suggested by Lima-de-Faria and Lopes-Vieira (36). Natural pyrolusite formed due to transformation from manganite exhibits (a) lamellar micropores 85 Å apart parallel to (010) (32–34), (b) zipper-like domains of either ramsdellite (34) or topotactic Mn_5O_8 (33) causing specific pyrolusite X-ray reflections to become diffuse. In contrast, manganite displays very sharp X-ray reflections thus the existence of significant groutite domains within the manganite precursor phase can be excluded. These observations are in better agreement with a transformation model of submicroscopic slip planes where the structural strain, due to the volume difference, is balanced by the formation of holes and ramsdellite (34) or Mn_5O_8 (33) domains which both require a smaller volume contraction. The evidence for a slip plane mechanism even for the closely related structures of manganite and pyrolusite suggests a similar model for the more complex groutite–pyrolusite transformation.

Klingsberg and Roy (39) have discovered an intermediate phase, tentatively named "groutellite," during the ramsdellite–groutite transformation. This phase with the possible composition Mn_2O_3OH (orthorhombic, *Pnma* setting, $a = 4.66$, $b = 2.87$, $c = 9.54$ Å) was confirmed by later experiments (1, 41). However, it is assumed (1) that groutellite does not appear in samples reduced far from equilibrium and that it does not form during the reverse reaction, i.e., oxidation of groutite to ramsdellite (39). The formation of this phase in the course of our groutite heating experiments below 300°C can rather be excluded. Upon heating, groutite X-ray reflections remained sharp and the intensity decreased only slightly as expected from increased thermal vibration. The *c*-axis of groutite increased homogeneously from 10.665 Å (25°C) to 10.773 Å (325°C) whereas formation of intermediate "groutellite" should yield a significant decrease of *c* to ca. 9.6 Å. Formation of groutellite has recently been suggested (1) during discharge of alkaline manganese dioxide batteries.

FTIR Spectroscopy on MnOOH Polymorphs

The subject of the following discussion are the peculiar absorption features around 2000 cm^{-1} in the IR spectra of manganite and groutite. Even though they might be treated as a sole, unique problem of MnOOH spectra, the authors are convinced that only consideration of, and comparison with similar features in the spectra of comparable M^{3+}OOH (M^{3+}OOD) compounds [M = Al, Fe, Ga, Sc, diaspore group (42); M = In, isotopological structure to manganite (30, 42); M = Co, Cr (43, 44)] provide a satisfactory solution. Moreover, previous discussions of similar features in "A, B, C"-type spectra (45, 46) of mostly organic substances with medium to strong hydrogen bonds, provide additional arguments. Thus, the band(s) around 2000 cm^{-1} in manganite and groutite may be explained by one of the following arguments which are grouped into three main categories:

1. Both of the bands around 2600–2700 and $\sim$2000 cm^{-1} are O–H stretching bands. Their existence can be explained in the following ways.

(A) Factor group splitting into two differently polarized components (see above) might lead to the two separated absorption features. *Counter argument*: A splitting amount of $\sim$600 cm^{-1} of the two normal modes which belong to the same internal coordinate (i.e., in-phase and out-of-phase stretching) has never been observed yet. Rather, there is good evidence that the two species are very closely split, and both are contained in the broad 2600–2700 cm^{-1} band. This is also supported by the polarization behavior.

(B) Schwarzmann *et al.* (47) suggested proton tunneling in a double minimum potential of the H-bond in manganite. Since the tunneling process, which may be described by dynamic H atom disorder, is in disagreement with the structure refinements, they proposed tunneling stimulated by the IR radiation during spectra acquisition. *Counter argument*: Even though a double minimum potential seems very likely in manganite (one minimum can be transformed into the other one by a simple twin transformation) their modeling is in poor agreement with the wide separation of the two bands. Further, IR spectra collected at different (and also very low) light intensities did not show any variations. Thus there is no evidence for a light-stimulated tunneling process.

(C) Inelastic neutron scattering spectra where modeled assuming a highly symmetrical position of the H atom in the structural channels of manganite (48). Similar suggestions were published by Kamath and Ganguly (49), who described MnOOH as a "bronze" of H and MnO_2 placing the H atoms in the center of the structural channels. *Counter argument*: The peak positions of their studies suggest that they used different or altered material but pure manganite. Their findings are in strong disagreement with a previous (7) and the present structure refinements, as well as with the fact that symmetrical H bonds are only observed at O–H···O distances below 2.5 Å.

(D) There might be two slightly different environments around the H atoms in manganite. The band positions around 2600–2700 and 2000 cm^{-1} indicate O–H···O distances of $\sim$2.60 (actually observed) and $\sim$2.55 Å (23). The latter might be produced by a distorted environment at the twin boundaries in manganite. *Counter argument*: The almost identical intensities of the two peaks are in disagreement with the comparably infrequent occurrence of the twin boundaries (refinement in a twin model instead of a disorder structure!). A study with the IR-microscope using a 50×50 μm aperture yielded identical spectra in differently twinned sections of a $4 \times 2 \times 0.004$ mm (100) manganite crystal section.

In addition, the following observations might be considered as a *general counter argument* of category 1: Upon deuteration (42) the two bands in manganite behave quite differently. Compared to the deuterated 2660 cm^{-1} band, the deuterated 2060 cm^{-1} band loses considerably intensity. The observed frequency shift of the 2660 cm^{-1} band ($\nu_{OH}/\nu_{OD} = 1.27$) is in good agreement with the "stretching frequency vs deuteration shift" correlation diagrams of Novak (23). In contrast, the 2060 cm^{-1} band yields a shift of $\sim$1.34 which deviates considerably from the value of $\sim$1.1 expected for short stretching frequencies. The observed shift rather suggests a bending mode.

At low temperatures (82 K) the bands around 2600–2700 cm^{-1} shift to shorter wavenumbers (Table 5) which is the usual behavior of stretching bands upon cooling. The bands around 2000 cm^{-1} shift to higher wavenumbers which is similar to the shift of the bending modes around 1000–1150 cm^{-1}. Finally, comparison with spectra of different M^{3+}OOH compounds (see above) suggests that the $\sim$2000 cm^{-1} bands are definitely not O–H stretching modes (detailed discussion below).

2. The two bands around 2600–2700 and $\sim$2000 cm^{-1} represent a single, broad OH stretching band interrupted by a minimum. This minimum can be explained in the following ways.

(A) The positions of the first overtones of the O–H bending modes (i.e., two times the wavenumbers of the in- and out-of-plane bending modes at $\sim$1000 to 1150 cm^{-1}) are in good agreement with the minimum between the 2600–2700 and $\sim$2000 cm^{-1} bands. Thus, the transmission "window" is caused by an overlap and Fermi resonance of these modes with the broad O–H stretching band (50). *Counter argument*: Due to the strong anharmonicity of strongly H-bonded O–H vibrations, the overtones must not be calculated by a simple multiplication. The real overtone positions are mostly shifted to lower wavenumbers (negative anharmonicity constant X!) than expected by a such simple calculation.

(B) Due to a very shallow potential surface, the ground state of the O–H stretching vibration might be completely depopulated by the IR radiation (comparable to laser absorption studies with high photon flux), thus yielding a minimum in the supposed broad band. *Counter argument*: Spectra acquired at different (and very low) light intensities did not result in different gap widths or depths. If the ground state is completely depopulated, absorptions at slightly lower wavenumbers (anharmonicity) due to the transition from the first to the second state ("hot bands") should be visible (51).

The appearance of more widely or closely separated peaks in comparable $Me^{3+}OOH$ spectra or the occurrence of very sharp component peaks at low temperatures may act as a *general counter argument* to the hypothesis stated above. This is also confirmed by the different behavior of the two component bands at low temperatures or upon deuteration (see discussion above).

3. The 2600–2700 cm^{-1} bands are the true, fundamental O–H stretching bands (related to the O–H···O distance of ~ 2.60 Å in the structures of manganite and groutite), and the $\sim 2000\ cm^{-1}$ band(s) are *not* stretching bands. However, as the strong shift upon deuteration of manganite shows, the latter are undoubtedly O–H modes.

(A) The bands around 2000 cm^{-1} represent additional bending modes. *Counter argument*: Even in short H bonds with low-frequency stretching modes, the bending modes do not exceed 1400 cm^{-1}. In addition, all bending modes allowed by factor group analysis have already been assigned to the 1000–1150 cm^{-1} group.

(B) The 2060 cm^{-1} band in manganite is a combination band of the OH-stretching mode at 2660 cm^{-1} and the excited lattice mode at 600 cm^{-1} (52). Thus, by 2660–600 = 2060, the position of the problematic band is accurately obtained. *Counter argument*: This combination works only in manganite, thus seems to be accidental. The contrarily oriented shift of the two peaks at low temperatures is no longer in agreement with this combination. According to normal mode analysis (factor group analysis in a crystal) the combination of an IR-active "*u*" mode (e.g., A_u, B_{1u}) with another "*u*" mode always yields a "*g*" mode (IR-forbidden) in a centrosymmetric crystal (53).

(C) The $\sim 2000\ cm^{-1}$ bands are combinations of the O–H stretching modes with low-wavenumber stretching modes (σ) of the whole O–H···O bonds. *Counter argument*: Since the latter is in the wavenumber region around 150 cm^{-1} it is rather suited to explain the broadening of the real stretching bands (46) than the existence of the widely separated $\sim 2000\ cm^{-1}$ bands.

(D) The bands around 2000 cm^{-1} might be "hot bands," i.e. transitions from the excited state to the doubly excited state of the stretching modes. *Counter argument*: A difference of $\sim 600\ cm^{-1}$ between normal and "hot band" can no longer be explained by anharmonicity. Hot bands usually become more intense at higher temperatures. This is opposite to the present observations.

(E) The $\sim 2000\ cm^{-1}$ bands represent combinations of an IR-active and Raman-active O–H bending mode. *Counter argument*: This is a weak argument, since the Raman modes cannot be proven due to the strong light absorption of the strongly colored MnOOH minerals. However, comparable Raman spectra of diaspore (42) did not support this hypothesis.

(F) The bands around 2000 cm^{-1} are the first overtone of the bending modes at 1000–1150 cm^{-1}. *Counter argument*: According to normal mode analysis (see above) the first overtones are IR-forbidden ($2 \times$ "*u*" = "*g*"). Further, the intensities (compared to the fundamental stretching and bending modes) are much too strong for an overtone.

Even though at least one counter argument can be found for each single hypothesis, the most probable explanation is given by group 3, which lacks a general counter criticism. Among this group, explanation 3F, an overtone of bending modes, is the most reasonable one. However, how can the counter arguments be handled seriously?

A thorough consideration of the behavior of medium to strong hydrogen bonds leads inevitably to the field of anharmonicity. A general review of this topic is given by Hadzi and Bratos (46) and Sandorfy (54). Which facts support the intimate relation of the $\sim 2000\ cm^{-1}$ bands to anharmonicity phenomena?

(a) The bands are strong in manganite and groutite but become less intense in diaspore, goethite, etc., which show weaker H bonding. It is well known that the anharmonicity of H bonds is generally very strong. Moreover, it increases dramatically with decreasing O–H···O distance and O–H stretching frequency (55).

(b) Compared to the real stretching bands around 2600–2700 cm^{-1}, the $\sim 2000\ cm^{-1}$ bands become much more intense at low temperatures. It is well proven that the anharmonicity increases with decreasing O–H···O distance at low temperature (54).

(c) In contrast, the $\sim 2000\ cm^{-1}$ band becomes much weaker and narrow upon deuteration. In $M^{3+}OOD$ compounds with weaker H bonds, the band disappears almost completely. It is well understood that the anharmonicity decreases with replacement of a constituent light atom by a heavier one (H/D).

(d) The position around 2000 cm^{-1}, which is lower than the expected values ($2 \times$ bending fundamental), confirms the strong anharmonicity (strong, negative anharmonicity constant X_{OH} (55)).

The counter arguments turn into supporting arguments if we consider the above mentioned facts. Moreover, in the case of strong anharmonicity, the overtone (forbidden by normal mode analysis) should appear according to local mode analysis. Normal mode analysis is only valid for harmonic vibrations or for cases in which a weak anharmonicity can

be treated by a simple perturbation theory. In the case of strong anharmonicity the normal mode analysis has to be replaced by local mode analysis (56, 57) which proved versatile in the interpretation of overtone spectra.

Finally, the high intensity of the overtone bands may be explained by anharmonicity resonance interaction (this seems to be a better term than "Fermi" resonance) with the main, broad O–H stretching band (46). The intensity of resonance increases with increasing H bond strength (increasing anharmonicity) and with approaching band positions. In addition, there is good evidence that the high-energy shoulder or peak (at low temperatures in groutite) around 2900 cm^{-1} is the resonance-enhanced second overtone of the bending modes under discussion. The peculiar, asymmetrical shapes of the overtone bands provide an additional supporting argument for resonance-enhanced intensities.

ACKNOWLEDGMENTS

This study was supported by the Swiss "Nationalfonds". Thanks are due to R. Oberhänsli for electron microprobe analysis of groutite, Ch. Hoffmann for help during the course of structure refinement, and M. Kunz for valuable discussions. We are indebted to G. R. Rossman for supporting this study with his FTIR equipment, for providing the diaspore samples, and for numerous helpful discussions. Financial support for the FTIR equipment came from the National Science Foundation, Grant EAR 9218980. E.L. is indebted to the "Fonds zur Förderung der wissenschaftlichen Forschung, Austria" for financial support during an "Erwin-Schrödinger" fellowship, Project J01098-GEO.

REFERENCES

1. Y. Chabre and J. Pannetier, *Prog. Solid State Chem.* **23,** 1–130 (1995).
2. P. M. de Wolff, *Acta Cryst.* **12,** 341–345 (1959).
3. L. A. H. MacLean and F. L. Tye, *J. Solid State Chem.* **123,** 150–160 (1996).
4. M. H. Rossouw, D. C. Liles, and M. M. Thackeray, *Mat. Res. Bull.* **27,** 221–230 (1992).
5. M. J. Garrido, *Bull. Soc. Franç. Minéral.* **58,** 224–241 (1935).
6. M. J. Buerger, *Z. Krist.* **95,** 163–174 (1936).
7. H. Dachs, *Z. Krist.* **118,** 303–326 (1963).
8. J. V. Smith, "Geometrical and structural crystallography" (J. V. Smith, Ed.), pp. 326–329. John Wiley & Sons, New York, 1982.
9. Y. D. Kondrashev and A. I. Zaslavsky, *Izv. Akad. Nauk SSSR, Ser. Fiz.* **15,** 179–186 (1951).
10. M. Pernet, C. Berthet-Colominas, M. A. Alario-Franco, and A. N. Christensen, *Phys. Status Solidi A* **43,** 81–88 (1977).
11. A. M. Byström, *Acta Chem. Scand.* **3,** 163–173 (1949).
12. J. W. Gruner, *Am. Mineral.* **32,** 654–659 (1947).
13. L. S. Dent Glasser and L. Ingram, *Acta Crystallogr., Sect. B* **24,** 1233–1236 (1968).
14. W. R. Busing and H. A. Levy, *Acta Crystallogr.* **11,** 798–803 (1958).
15. "Structure determination package (SDP)." Enraf Nonius, Delft, The Netherlands, 1983.
16. G. M. Sheldrick, "SHELX93, Program for crystal structure determination." University of Göttingen, Germany, 1993.
17. Siemens, "XLS/SHELXTL PC, Release 4.1." Siemens Analytical X-Ray Instruments, Inc., Madison, WI, 1991.
18. R. D. Shannon, M. A. Subramanian, A. N. Mariano, T. E. Gier, and G. R. Rossman, *Am. Mineral.* **77,** 101–106 (1992).
19. E. Libowitzky and G. R. Rossman, *Am. Mineral.* **81,** 1080–1091 (1996).
20. E. Schwarzmann and H. Marsmann, *Z. Naturforsch.* **21B,** 924–928 (1966).
21. R. M. Potter and G. R. Rossman, *Am. Mineral.* **64,** 1199–1218 (1979).
22. D. M. Adams and D. C. Newton, "Tables for factor group and point group analysis." Beckman-RIIC Limited, Croydon, England, 1970.
23. A. Novak, *Struct. Bonding* **18,** 177–216 (1974).
24. A. Szytula, A. Burewicz, Z. Dimitrijewic, S. Krasnicki, H. Rzany, J. Todorovic, A. Wanic, and W. Wolski, *Phys. Status Solidi* **26,** 429–434 (1968).
25. A. A. Bolzan, C. Fong, B. J. Kennedy, and C. J. Howard, *Aust. J. Chem.* **46,** 939–944 (1993).
26. A. N. Christensen, *Acta Chem. Scand.* **18,** 1261–1266 (1964).
27. A. N. Christensen, *Inorg. Chem.* **5,** 1452–1453 (1966).
28. J. Chenavas, J. C. Joubert, J. J. Capponi, and J. Marezio, *J. Solid State Chem.* **5,** 1–15 (1973).
29. I. D. Brown, *Acta Crystallogr. Sect. A* **32,** 24–31 (1976).
30. M. S. Lehmann, F. K. Larsen, F. R. Poulsen, A. N. Christensen, and S. E. Rasmussen, *Acta Chem. Scand.* **24,** 1662–1670 (1970).
31. D. R. Dasgupta, *Min. Mag.* **35,** 131–139 (1965).
32. P. E. Champness, *Min. Mag.* **38,** 245–248 (1971).
33. J. H. Rask and P. R. Busek, *Am. Mineral.* **71,** 805–814 (1986).
34. N. Yamada, M. Ohmasa, and S. Horiuchi, *Acta Cryststallogr. Sect. B* **42,** 58–61 (1986).
35. M. Ripert, C. Poinsignon, Y. Chabre, and J. Pannetier, *Phase Transitions* **32,** 205–209 (1991).
36. J. Lima-de-Faria and A. Lopes-Vieira, *Min. Mag.* **33,** 1024–1031 (1964).
37. L. S. Dent Glasser and I. B. Smith, *Min. Mag.* **35,** 327–334 (1965).
38. R. Giovanoli, and U. Leuenberger, *Helv. Chim. Acta* **52,** 2333–2347 (1969).
39. C. Klingsberg and R. Roy, *Am. Mineral.* **44,** 819–838 (1959).
40. B. G. Hyde and S. Andersson, "Inorganic crystal structures" (B. G. Hyde and S. Andersson, Eds.). John Wiley & Sons, New York, 1989.
41. L. S. Dent Glasser and I. B. Smith, *Min. Mag.* **36,** 976–987 (1968).
42. E. Schwarzmann, and H. Sparr, *Z. Naturforsch.* **24B,** 8–11 (1969).
43. R. G. Delaplane, J. A. Ibers, J. R. Ferraro, and J. J. Rush, *J. Chem. Phys.* **50,** 1920–1928 (1969).
44. R. G. Snyder and J. A. Ibers, *J. Chem. Phys.* **36,** 1356–1360 (1962).
45. Y. I. Ryskin, "The infrared spectra of minerals" (V. C. Farmer, Ed.), pp. 137–181. Mineralogical Society, London, 1974.
46. D. Hadzi and S. Bratos, "Structure and spectroscopy" (P. Schuster, G. Zundel, and C. Sandorfy, Eds.), Vol. II, pp. 565–611. North-Holland, Amsterdam, 1976.
47. E. Schwarzmann, O. Glemser, and H. Marsmann, *Z. Naturforschung* **21B,** 1128–1131 (1966).
48. F. Fillaux, C. H. Cachet, H. Ouboumour, J. Tomkinson, C. Lévy-Clément, and L. T. Yu, *J. Electrochem. Soc.* **140,** 585–591 (1993).
49. P. V. Kamath and S. Ganguly, *Mater. Lett.* **10,** 537–539 (1991).
50. M. F. Claydon and N. Sheppard, *Chem. Commun.* **23D,** 1431–1433 (1969).
51. H. Graener, *J. Phys. Chem.* **95,** 3450–3453 (1991).
52. C. Cabannes-Ott, *Ann. Chim. Ser. 13*, **5,** 905–960 (1960).
53. E. B. Wilson, J. C. Decius, and P. C. Cross, "Molecular vibrations" (E. B. Wilson, J. C. Decius and P. C. Cross, Eds.), p. 388. Dover Publications, Inc., New York, 1980.
54. C. Sandorfy, "Structure and spectroscopy" (P. Schuster, G. Zundel, and C. Sandorfy, Eds.), Vol. II, pp. 613–654. North-Holland, Amsterdam, 1976.
55. H. D. Lutz and M. Schmidt, *Spectrosc. Acta* **47A,** 585–594 (1991).
56. M. S. Child and L. Halonen, *Adv. Chem. Phys.* **57,** 1–58 (1984).
57. I. M. Mills and A. G. Robiette, *Mol. Phys.* **56,** 743–765 (1985).